JACS
JOURNAL OF THE AMERICAN CHEMICAL SOCIETY
Article
pubs.acs.org/JACS

Highly Twisted *N,N*-Dialkylamines as a Design Strategy to Tune Simple Aromatic Hydrocarbons as Steric Environment-Sensitive Fluorophores

Shunsuke Sasaki,[†] Satoshi Suzuki,[‡] W. M. C. Sameera,[‡] Kazunobu Igawa,[§] Keiji Morokuma,*[,‡] and Gen-ichi Konishi*[,†,⊥]

[†]Department of Organic and Polymeric Materials, Tokyo Institute of Technology, Tokyo 152-8552, Japan
[‡]Fukui Institute for Fundamental Chemistry, Kyoto University, Kyoto 606-8103, Japan
[§]Institute for Materials Chemistry and Engineering, Kyushu University, Fukuoka 816-8580, Japan
[⊥]PRESTO, Japan Science and Technology Agency (JST), Tokyo 102-0076, Japan

Supporting Information

ABSTRACT: The steric-environment sensitivity of fluorescence of 9,10-bis(*N,N*-dialkylamino)anthracenes (**BDAAs**) was studied experimentally and theoretically. A new design strategy to tune simple aromatic hydrocarbons as efficient aggregation-induced emission (AIE) luminogens and molecular rotors is proposed. For a variety of **BDAAs**, prominent Stokes shifts and efficient solid-state fluorescence were observed. Calculations on **BDAA-methyl** suggested that in the ground state (S_0) conformations, the pyramidal amine groups are highly twisted, so that their lone-pair orbitals cannot conjugate with the anthracene π orbitals. Fluorescence takes place from the S_1 minima, in which one or both amine groups are planarized. The stability of the S_1 excited state minima as well as destabilization of the S_0 state is the origin of large Stokes shift. Experimental measurement of the nonadiabatic transition rate suggests that *para* disubstitution by dialkylamino (or strongly electron-donating) groups is a key for fast internal conversion. Minimum energy conical intersection (MECI) between S_1 and S_0 states was found to have a Dewar-benzene like structure. Although this can be reached efficiently in liquid phase for fast internal conversion, a large amplitude motion is required to reach this MECI, which is prohibited in the solid state and caused efficient AIE. This strategy is used to find experimentally that naphthalene analogues are also efficient AIE luminogens. The flexibility of alkyl chains on amino groups is also found to be important for allowed charge-transfer transition. Thus, three points [(1) highly twisted *N,N*-dialkylamines, (2) substitution at the *para* positions, (3) with flexible alkyl groups] were proposed for activation of small aromatic hydrocarbons.

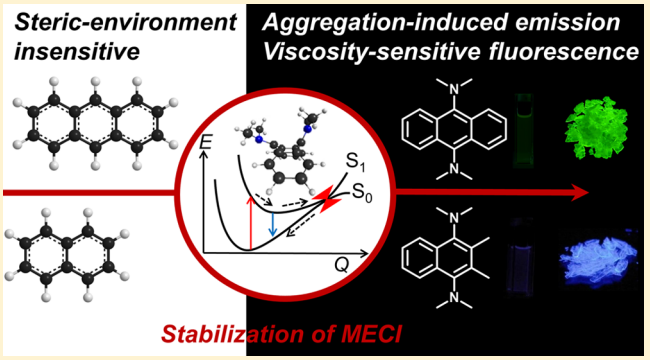

INTRODUCTION

Fluorescent molecules are sensitive to their steric environments, such as local viscosities, aggregations, binding to macromolecules and encapsulations to cavities. These fluorescent molecular systems have recently emerged as versatile imaging/detection materials for molecular biology,[1−4] polymer science,[5,6] supramolecular chemistry,[7,8] contact mechanics[9] and fluid dynamics.[10] Fluorescent molecular rotors[11] and aggregation-induced emission luminogens (AIEgens)[12] are representative types of steric-environment sensitive fluorophores, as they exhibit sizable changes in fluorescence intensity, lifetime, and spectral shape in response to subtle steric restrictions.

Commonly used fluorophores undergo straightforward emission from an excited state (Figure 1a), while fluorescent molecular rotors and AIEgens are designed to involve much more complicated relaxation paths. Their surrounding steric environments affect the excited-state equilibrium (Figure 1b) and/or internal conversion rate (Figure 1c). Most of the fluorescent molecular rotors[11,13,14] and several AIEgens[15] possess strong donor−acceptor (D−A) structures to utilize their excited-state equilibrium, often called the "twisted intramolecular charge transfer" (TICT) state.[16] In sterically restricted environments, interconversion between a weakly fluorescent TICT state and highly fluorescent states (e.g., locally excited (LE) or "coplanar" ICT states) is hampered, resulting enhanced fluorescence intensity and deformed spectral shape (Figure 1b). On the other hand, inhibition of internal conversion, by restricting intramolecular motions (RIM), is the principal design strategy of AIEgens. Fast internal conversion can be induced by vibration in solution,[17] but is suppressed in solid states (Figure 1c).[12] Since isomerizable

Received: April 20, 2016
Published: June 14, 2016

ACS Publications © 2016 American Chemical Society

DOI: 10.1021/jacs.6b03749
J. Am. Chem. Soc. 2016, 138, 8194−8206

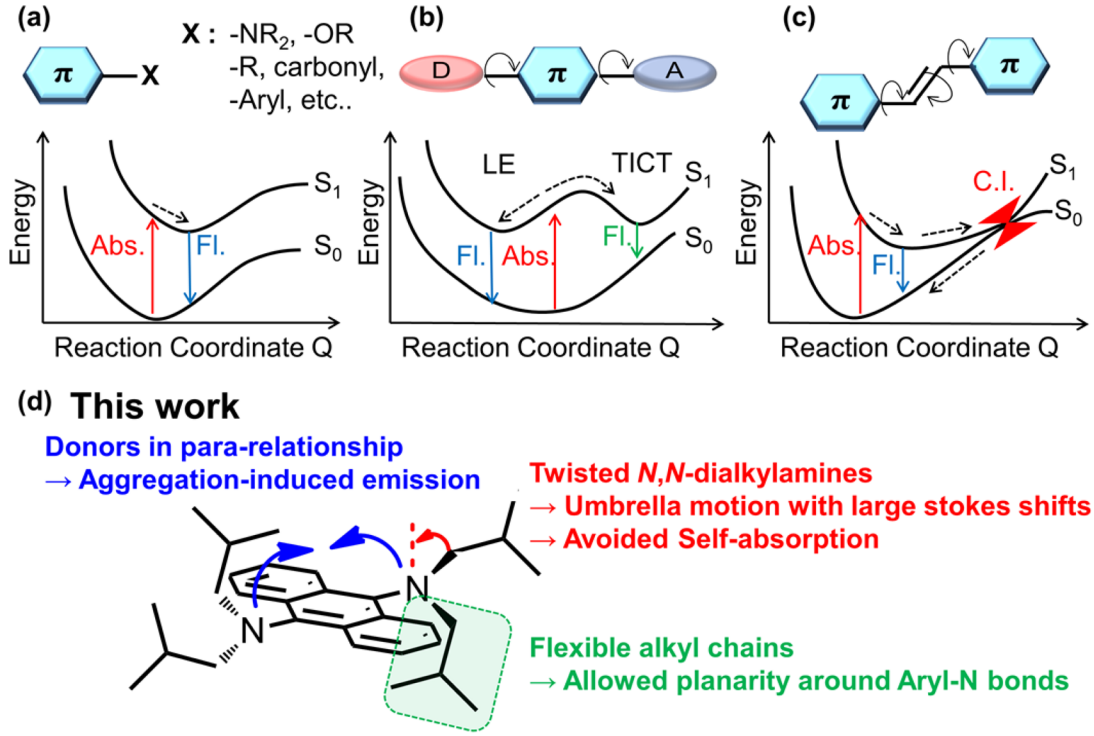

Figure 1. Typical potential energy surfaces of classic and steric-environment sensitive fluorophores. (a) "Matched" potential surfaces of typical aromatic hydrocarbons, (b) potential surfaces with "double-minima" of strong donor–acceptor systems, (c) potential surfaces with a conical intersection, and (d) the design strategy revealed by this work.

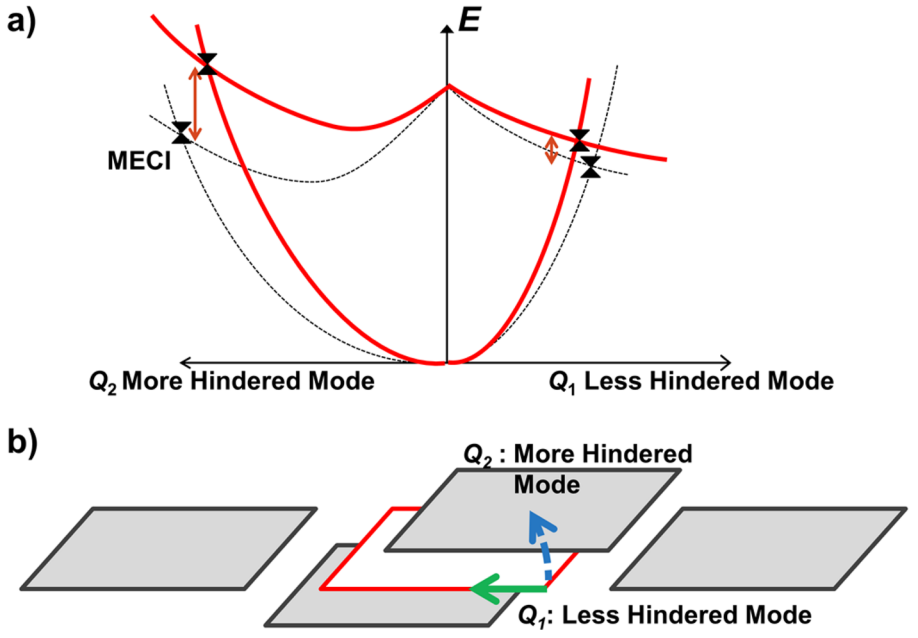

Figure 2. (a) Schematic illustration of potential energy surfaces in solid. Black broken lines are PESs in gas phase. Red solid lines are PESs in solid. (b) Some motions (illustrated by blue arrow) will be hindered by the surroundings but others (in green arrow) may still be unhindered.

double bonds[18] and multiple aryl–aryl bonds[19] often dominate such vibrations, these structures have been adopted in many AIEgens. In spite of recent advances in the area, it is still challenging to develop fluorophores from simple aromatic hydrocarbons that are sensitive to steric environments. Simple aromatic hydrocarbons, such as benzene, naphthalene and anthracene, do not undergo any excited-state reaction within lower singlet manifolds, and introduction of either donor or acceptor on these hydrocarbons do not improve this problem. Therefore, development of novel strategies that modifies the potential energy surfaces (PESs) of the aromatic hydrocarbons to undergo excited-state reactions becomes critical.

Herein, we propose highly twisted *N*,*N*-dialkylamine as an "activating group" that modifies the PESs of typical aromatic hydrocarbons. Commonly used *N*,*N*-dialkylaminoarenes do not undergo excited-state reactions such as TICT formation, as

DOI: 10.1021/jacs.6b03749
J. Am. Chem. Soc. 2016, 138, 8194–8206

Scheme 1

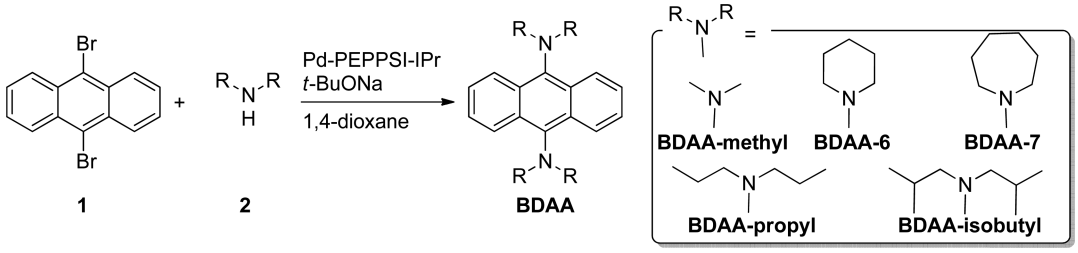

they do not have strong electron withdrawing groups. However, once an *N*,*N*-dialkylamino group is twisted, several intriguing phenomena related to steric environments can take place. Warner et al. found strong viscosity dependence of fluorescence intensity and spectral shape for 9-(*N*,*N*-dimethylamino)-anthracene.[20] They concluded that the sensitivity toward viscosity stems from the excited-state equilibrium between the ^1L_a state localized on anthracene and the ^{1}CT state accompanied by planarization around the aryl-N bonds. We have recently examined AIE characteristics for various regioisomers of mono- and bis(piperidyl)anthracenes, and found that only 1,4- and 9,10-substitution brought drastic AIE effects.[21] Our preceding experimental studies revealed that **BDAA-6** was not subjected to excitonic interactions even in solid state.[21] Nevertheless, these studies did not address the key questions; how does the *N*,*N*-dialkylamino group make the anthracene ring highly fluorescent only in viscous media and solid states?

From theoretical point of view, the fluorescence quantum yield is related to competition between emission and quenching. Quenching is caused by internal conversion of electronic energy to internal energies by nonadiabatic transition from one electronic state to another. Internal conversion is likely to take place when the energy difference between two electronic states is small. The points where two electronic states (of the same spin multiplicity) have the same energy (degenerate) are called the conical intersection (CI).[22] When *f* is the internal degree of the system, the CI occurs in *f*-2 dimension; the CI is not just a point but is an *f*-2-dimensional hypersurface. The minimum energy conical intersection (MECI) is the lowest point on CI hypersurface. Below this energy internal conversion cannot take place efficiently. The geometry and energy of MECI should play a very important role in internal conversion.

Therefore, designing geometry and energy of MECI is a promising strategy for controlling internal conversion. If the MECI is higher than the Franck−Condon energy, it is difficult to reach any point on conical intersection hypersurface, and therefore the molecule is likely to be emissive. One key of AIE is that the environment restricts some vibrational motions of a molecule. If a molecule has a MECI that has a large geometry change from the Franck−Condon geometry, the molecule would be able to reach the MECI in liquid, but not in solid where surroundings are likely to raise the energy of MECI that is associated with a large distortion (Figure 2). If all motions toward the conical intersection are inhibited by the surroundings, internal conversion will not take place and the molecule will become emissive. Similar ideas have also shown by us and others about conical intersection in solid.[23−25] We will go a little further by using these areas for design strategy of the present systems.

In order to describe electronic structure in the vicinity of the conical intersection correctly, the wave functions of the two states need to be described on equal footing. The multi-configuration self-consistent field (MCSCF) method is a standard method to achieve the requirement. The complete active space self-consistent field (CASSCF) method is the most common variation of the MCSCF method, taking all possible combination of electronic configurations within the active space defined by a set of orbitals and electrons. Once the wave function is obtained, there are many techniques to find MECIs based on a constrained optimization method, such as the penalty function method,[26] the gradient projection method[27] and the updated branching plane method.[28] In the present work, we will use the gradient projection method.

In this study, we have experimentally and theoretically investigated steric effects on photophysical properties of bis(*N*,*N*-dialkylamino)anthracenes (**BDAA**s, Figure 1d). Our results demonstrate that highly twisted *N*,*N*-dialkylamino groups tune anthracene for fluorescence in two ways. (1) Torsion around the aryl-nitrogen bonds causes unique structural relaxation, giving rise to large Stokes shifts, and (2) *para* disubstitution on **BDAA**s by diamines promotes the internal conversion via conical intersection in solution, but retains strong fluorescence in solid. This unveiled mechanism is then applied to design novel AIEgens comprised of a single naphthalene ring, i.e., **DMe-DAN** and **DMe-BDAN** (see below). Additionally, our photophysical measurements and theoretical approach revealed the effect of alkyl-chain flexibility; a large but flexible *N*,*N*-dialkylamino group, such as *N*,*N*-diisobutylamino, is more likely to make the aryl-nitrogen bond of **BDAA**s coplanar than a small and stiff group such as *N*,*N*-dimethylamino.

EXPERIMENTAL METHODOLOGY

Photophysical Measurements of Solid Samples. Prior to any photophysical measurements of solid states, i.e., polycrystalline solids, colloidal suspensions (THF:water = 1:9 (v/v)), and dispersion in NaBr, recrystallization and subsequent fluorescence quantum yield measurements were repeated three times. First, polycrystalline solids were recrystallized from chloroform−hexane mixed solvent, then from ethyl acetate, and finally from ethanol at −10 °C. In the realm where **BDAA**s possess significant absorbance, fluorescence quantum yields were almost independent to excitation wavelength. Besides, fluorescence quantum yields after the third recrystallization was seldom changed from that after the second recrystallization (Figure S1−S2). Taking these facts into accounts, we regarded polycrystalline solid obtained from the third recrystallization is sufficiently pure to discuss photophysical properties.

Typical domain sizes of the polycrystalline solids were around 10 μm to 1 mm (Figure S3−S7). These polycrystalline solids were used for preparations of colloidal suspensions and dispersions in NaBr (see Section S1).

DOI: 10.1021/jacs.6b03749
J. Am. Chem. Soc. 2016, 138, 8194−8206

Scheme 2

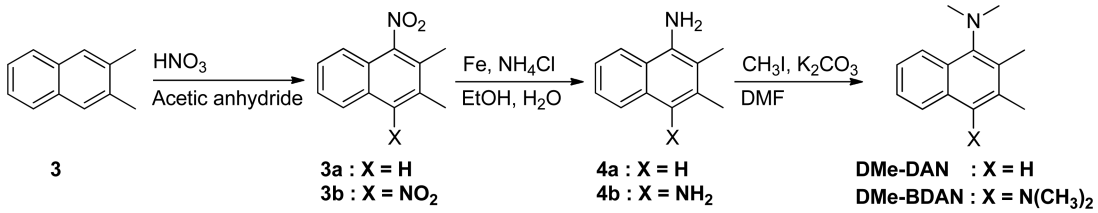

Since **BDAN**, **DMe-DAN** and **DMe-BDAN** are too soluble to common organic solvents, recrystallizations were conducted only with ethanol or methanol. For the same reason, aggregations of these compounds were not observed in THF:water = 1:9 (v/v) and AIE effects were evaluated only with polycrystalline solids.

As reported in our previous research,[21] diffuse-reflectance spectra (Figure S8) were recorded on JASCO FP-6500 spectrofluorometer to monochromate outgoing lights. Detailed procedures are summarized in the Supporting Information (Section S1–S2).

Synthesis and Characterization. 9,10-Bis(piperidyl)anthracene (**BDAA-6**), 9,10-bis(hexamethyleneimino)anthracene (**BDAA-7**), 9,10-bis(*N*,*N*-dipropylamino)anthracene (**BDAA-propyl**) and 9,10-bis(*N*,*N*-diisobutylamino)anthracene (**BDAA-isobutyl**) were synthesized by Pd-catalyzed carbon–nitrogen coupling reactions using $Pd(OAc)_2$/BINAP[29] or Pd-PEPPSI-IPr[30] catalyst systems (Scheme 1). Due to their high reaction temperature, volatile *N*,*N*-dialkylamines, such as *N*,*N*-dimethylamine are not suitable for the coupling reactions. **BDAA-methyl** was synthesized via the conventional route,[31] where the synthetic intermediate 9,10-diaminoanthracene was subjected to rapid oxidation[32] and **BDAA-methyl** was therefore yielded only at 5% from the starting materials. We have also examined coupling reactions with further bulky *N*,*N*-dialkylamines (i.e., *N*,*N*-diisopropylamine, *N*,*N*-dicyclohexylamine) adopting Pd-PEPPSI-IPr, $Pd(OAc)_2$/BINAP, RuPhos[33] and P(*t*-Bu)$_3$[34] catalyst systems and *n*-butyllithium as a strong base.[35] These systems however ended up in debromination of aryl bromides.

For naphthalene series, coupling of 1,4-dibromo-2,3-dimethylnaphthalene with *N*,*N*-dialkylamines was not proceeded at all. Thus, novel compounds, 1-(*N*,*N*-dimethylamino)-2,3-dimethylnaphthalene (**DMe-DAN**) and 1,4-bis(*N*,*N*-dimethylamino)-2,3-dimethylnaphthalene (**DMe-BDAN**), were synthesized by the Friedel–Crafts nitration[36] and subsequent reduction and permethylation (Scheme 2). 1-(*N*,*N*-dimethylamino)naphthalene (**DAN**) and 1,4-bis(*N*,*N*-dimethylamino)naphthalene (**BDAN**) were prepared following the reported procedure.[37] All compounds were characterized by ^{1}H NMR, ^{13}C NMR (Figure S9–S30) and FT-IR. Melting point measurements were conducted for those with the melting points above the room temperature. Novel compounds were also characterized by high-resolution mass spectra (HRMS). Detailed synthetic procedures and characterization data were compiled in Supporting Information (Section S3).

COMPUTATIONAL METHODOLOGY

Geometry Optimization of BDAA-methyl. Geometries of **BDAA-methyl** in the ground state S_0 and in the lowest singlet excited state S_1 were optimized with the density functional theory (DFT) and time-dependent density functional theory (TDDFT), respectively, as implemented in the Gaussian 09 package.[38] At first, two local minima on the ground state were obtained at the B3LYP/6-31+G(d) level. These two are rotamers, one belongs to C_{2v} symmetry (*syn*), and the other in C_{2h} symmetry (*anti*). C_{2h} structure is the global minimum. Starting from the C_{2h} structure, the S_1 geometry was optimized at the TD-B3LYP/6-31+G(d) level.

Conical Intersection Optimization of BDAA-methyl. The minimum energy conical intersection (MECI) of **BDAA-methyl** was optimized at the two-state-averaged (2sa-)CASSCF/6-31G(d) level. Active space was defined using the Pipek–Mezey localized HF orbitals. Two nitrogen lone-pairs and 6π electrons in 6π orbitals located at the central ring were used as the active space, resulting in the (10e,8o)CAS. The gradient projection method implemented in GAMESS[39] was employed to find the MECI. The single point energies of S_0 to S_4 states were calculated at the (4sa-)CASSCF/6-31G(d) level.

Conformational Analysis of BDAA-isobutyl and BDAA-6. To see what makes a large difference in absorption spectra of **BDAA** with different alkyl groups, conformers of **BDAA-isobutyl** and **BDAA-6** were obtained by the following scheme. At first, conformational analysis were performed by the Tinker7.0 program[40] with the MM3 force field.[41] Using conformers found above, geometries were optimized with B3LYP-D3/6-31G(d) using Gaussian 09 program, including PCM solvation treatment with toluene.

RESULTS AND DISCUSSION

Aggregation-Induced Emission. Regardless of alkyl groups, all of **BDAA**s exhibit sizable AIE (Table 1). Especially

Table 1. Fluorescence Quantum Yields Φ_f of BDAAs in Toluene Solutions and Polycrystalline Solids

entry	toluene solution	polycrystalline solids
BDAA-methyl	0.006	0.702
BDAA-6	0.024	0.856
BDAA-7	0.099	0.252
BDAA-propyl	0.262	0.908
BDAA-isobutyl	0.078	0.914

polycrystalline solids of **BDAA-methyl**, **BDAA-6**, **BDAA-propyl**, and **BDAA-isobutyl** mark prominent fluorescence quantum yields (Φ_f = 0.70–0.98) compared to reported simple AIEgens.[14,42,43] Such a bright AIE was not observed for other regioisomers, i.e., 1-, 2-piperidylanthracenes and 1,5-, 1,8-, 2,6-bis(piperidyl)anthracenes, for which fluorescence was severely quenched upon aggregation.[21] 1,4-Bis(piperidyl)anthracene also exhibited weak AIE, and fluorescence quantum yield in polycrystalline state is 0.49. In our previous research,[21] we could not account for the paradox between efficient solid-state fluorescence of **BDAA-6** and their dense and face-to-face packing. In the same way, other **BDAA**s in this study are densely packed within several Å range (Figure 3a–e), but their diffuse-reflectance (Figure S8) and fluorescence spectra in colloidal suspensions, NaBr dispersions, and polycrystalline solids (Figure S31–S33) did not show any sign of intermolecular excitonic interactions. In the present contribution, a detailed photophysical study and theoretical calculations explained the answers for this paradox (vide infra). To achieve better performing AIEgen, a molecule has to show the following features: (1) small self-absorption in solid, and (2) fast quenching in liquid. The small self-absorption is closely related the large Stokes shift. The fast quenching is controlled by the internal conversion. In the following section, we discuss why **BDAA**s show AIE based on these two criteria.

DOI: 10.1021/jacs.6b03749
J. Am. Chem. Soc. 2016, 138, 8194–8206

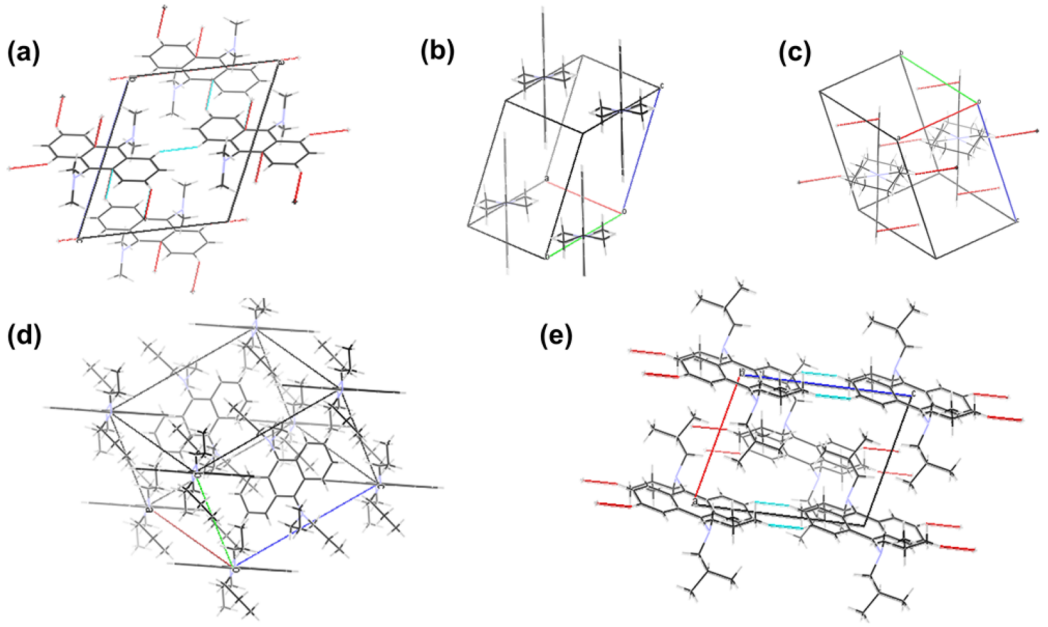

Figure 3. X-ray crystallographic structure of (a) **BDAA-methyl**, (b) **BDAA-6**, (c) **BDAA-7**, (d) **BDAA-propyl**, and (e) **BDAA-isobutyl**. Red and blue lines express short contacts within sum of van der Waals radii. ORTEP drawings are compiled in Figure S42–S46.

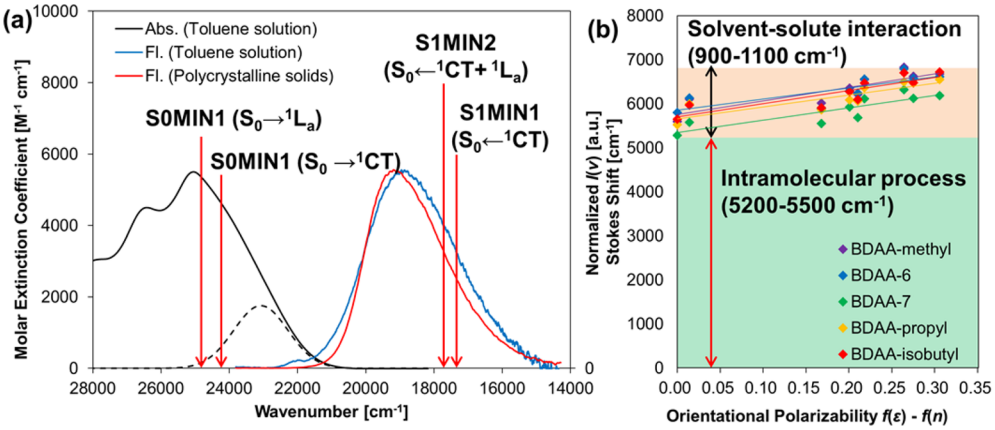

Figure 4. (a) absorption (Abs.) and fluorescence (Fl.) spectra of **BDAA-methyl** (inset: excitation energy of each transition was indicated as a red arrow); (b) Lippert–Mataga plots[46] against orientational polarizability $f(\varepsilon) - f(n) = (\varepsilon - 1)/(2\varepsilon + 1) - (n^2 - 1)/(2n^2 + 1)$, where n and ε are the refractive index[47] and dielectric constant,[47] respectively.

Large Experimental Stokes Shift. All BDAAs show large Stokes shifts (5200–6700 cm^{-1}, see Table S1 and Figure S34–S35 for detail) that are comparable with the recently reported dyes designed to possess large Stokes shifts.[44,45] Furthermore, the large Stokes shift was retained even in polycrystalline solids (Figure 4a, see Table S2 for other **BDAAs**). In the Lippert–Mataga plot[46] (Figure 4b), the Stokes shifts are ascribed mainly to intramolecular process, and therefore some excited-state conformational changes are likely to be involved.

Conformations in the Ground and S_1 States. Computed potential energy profiles of **BDAA-methyl** are discussed in this section. Figure 5 (also Table S5, Figure S47) shows the potential energy profiles as functions of two pyramidal angles, θ and θ', for the ground S_0 and the first excited S_1 state. The relevant structures of local minima are also included. The ground state potential energy surface has two minima; one is *anti* (S0MIN1) and the other is *syn* (S0MIN2) with respect to the two pyramidal amine ($N(CH_3)_2$) groups. This can be envisioned by taking a Newman projection with respect to the two amine nitrogen atoms, and keeping the anthracene ring placed horizontally as shown in Figure 5, where *syn* and *anti* indicate these S_0 minimum structures. As shown in Table 2, the amine pyramidal angles, θ in the front and θ' in the back, are both 146.1° for the *anti* minimum (S0MIN1), while θ is 146.6° and θ' is 213.4° for the *syn* minimum (S0MIN2). S0MIN1 structure is slightly more stable, where the energy difference is only 0.5 kJ/mol at B3LYP/6-31+G(d) level. The transition state between *anti* and *syn* forms (S0TS, Table 2) for *inversion* of the one amine group (θ' = 180.0°), retaining the other pyramidal amine (θ = 146.8°), is only 10.3 kJ mol^{-1} above S0MIN1. The energy difference between two minimum conformations as well as the height of inversion barrier is small, and therefore S0MIN1 and S0MIN2 can coexist at the room temperature.

On the other hand, it should be emphasized that the barrier for *rotation* of an amine between S0MIN1 and S0MIN2 is much higher (about 54 kJ mol^{-1}) and needs not be considered. This is because of the large repulsion between the amine

DOI: 10.1021/jacs.6b03749
J. Am. Chem. Soc. 2016, 138, 8194–8206

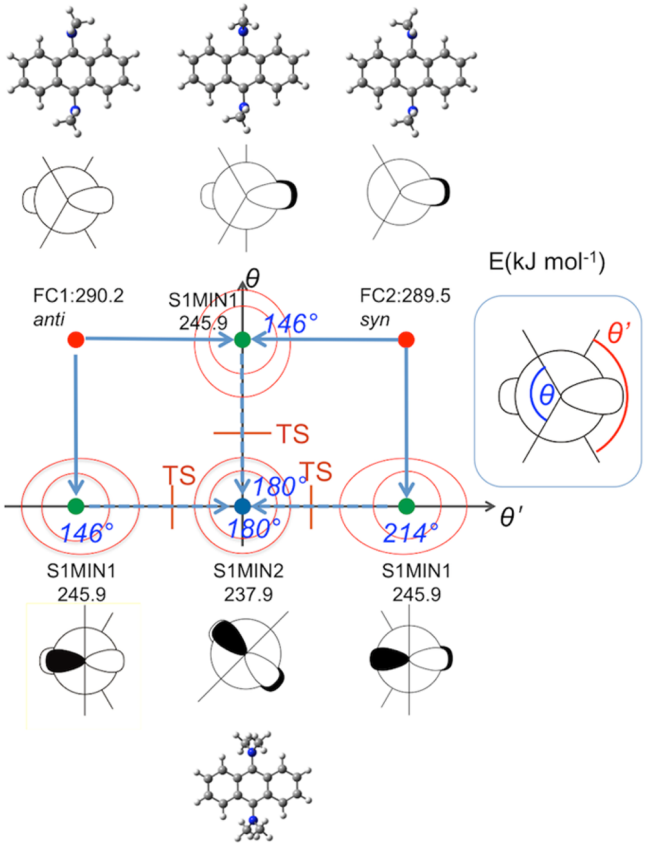

Figure 5. Schematic illustration of S_1 potential energy surfaces of **BDAA-methyl** at the TD-B3LYP/6-31+G(d)level. Structures of ground state minima (**S0MIN1**, i.e., *anti* or **FC1** and **S0MIN2**, i.e., *syn* or **FC2**), and excited state minima (**S1MIN1** and **SIMIN2**) are explicitly shown. The Newman projection is with respect to the nitrogen−nitrogen axis, and with the anthracene ring placed horizontally. White and black lobes signify the nitrogen lone-pair orbitals, and methyl groups on nitrogen are represented by adjacent lines.

Table 2. Optimized Structures (Dihedral Angles in °) of the Local Minima and Transition States of S_0 and S_1 States of BDAA-methyl at the TD-B3LYP/6-31+G(d) Level[a]

	θ	φ	θ'	φ'	
S0MIN1	146.07	0.00	146.07	0.00	C_{2h}
S0MIN2	146.59	180.00	213.41	0.00	C_{2v}
S0TS	146.78	0.00	180.02	0.00	C_s
S1MIN1	179.91	0.00	147.13	0.00	C_s
S1MIN2	180.00	31.1	180.00	31.1	C_{2h}

[a]Optimized structure in Table S7−S10.

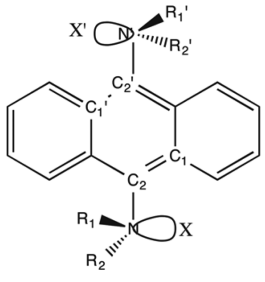

$\varphi = \angle C_1\, C_2\, N\, X$

$\varphi' = \angle C_1'C_2'N'X'$

$\theta = \angle R_1N\, C_2\, R_2$

$\theta' = \angle R_1'\, N'\, C_2'\, R_2'$

methyl groups and the anthracene *peri*-hydrogens, which cannot be avoided during the rotation.

In the S0MIN structures, both amine lone-pairs are perpendicular to the anthracene π orbitals (φ = 0°), and do not conjugate with anthracene. At both of these structures, the absorption is allowed with large oscillator strength and takes the molecule to the S_3 $\pi \rightarrow \pi^*$ states, the ^1L_a states in Platt's notation.[48] These S_3 states are higher than the S_1 states by only 8−9 kJ mol^{-1} (See Table 3).

Upon absorption of energy, the molecule is excited to the S_3 Franck−Condon (FC) structures, and then expected to come down to the lowest S_1 state.[49] As seen in Figure 5, both *anti* and *syn* FC structures on S_1 will relax without a barrier to S1MIN1, a minimum on S_1. S1MIN1 has a structure with one pyramidal amine group (θ = −147.0°) and the other planar amine group (Table 3), and this is very similar to S0TS. From the *anti* FC structure, two equivalent pathways exist, leading to two equivalent S1MIN1s. As a result of this, planarizing either the front amine group or the back amine group takes place. At the S1MIN1 structure, the S_1 state is a charge-transfer dominant state (^{1}CT, or n $\rightarrow \pi^*$, Table 3).

In addition, we have found a different type of conformer in the S_1 state, namely S1MIN2, which is lower than S1MIN1 by 7.6 kJ mol^{-1}. In S1MIN2 both amines became planar and are rotated by about φ = 31.1° (Figure S52). Now the amine lone-pairs can conjugate with the anthracene π orbitals (Table 3). As shown in Figure 5, there should be four transition states connecting S1MIN2 to four equivalent S1MIN1s. (Figure 5 shows only three, as the fourth one is symmetrically equivalent and is located in the section below the illustrated section.) We did not locate this barrier, as preliminary calculations suggested that this is low and not essential to photochemistry. The excited molecule that came down to S_1 FC structures is 290 kJ mol^{-1} above the ground state, and it would be able to access both S1MIN1 and S1MIN2. At the S1MIN2 structure, the S_1 state has a mixed character of ^{1}CT and locally excited ^1L_a state (Table 3).

We should emphasize that the present deformation in S1MIN1 and S1MIN2 is totally different from that of the famous TICT molecule 4-(*N*,*N*-dimethylamino)benzonitrile (DMABN),[16] In DMABN, the ground state planar amine is coplanar with the aromatic ring and its lone-pair conjugates with the aromatic π orbitals. In the S_1 state, the amine rotates and its lone-pair becomes orthogonal to the π aromatic ring. The aryl-nitrogen rotation angle, φ, is the principle reaction coordinate. On the other hand, in the case of **BDAA**s, the "pyramidal and non-conjugative (φ = 0°)" amines in the ground state minima become "planar and non-conjugative" in the S1MIN1 structure or "planar and conjugative (leaned, $\varphi \sim$ 31°)" in the S1MIN2 structure. In **BDAA**s, the severe steric repulsion from anthracene *peri*-hydrogens prohibits the aryl-nitrogen rotation of the pyramidalized dialkylamines, and the "umbrella inversion" motion of the alkylamines becomes the principal reaction coordinate. The effects of alkyl chain flexibility will be discussed again in a later section.

Calculated Stokes Shift. Fluorescence frequencies of **BDAA-methyl** from S1MIN1 and S1MIN2 are calculated at the TD-B3LYP/6-31+G(d) level as 17400 and 17600 cm^{-1}, respectively (Table 3), corresponding to a large Stokes shift of 6700−6900 cm^{-1}. This Stokes shift agrees well with the experimental value of 5200−6700 cm^{-1} (Figure 4b). Table 3 shows that this large Stokes shift of 80−82 kJ mol^{-1} originates in part from the stabilization of the S_1 excited state in the geometry change from structure S0MIN1 or S0MIN2 to S1MIN1 (38 kJ mol^{-1}) or S1MIN2 (28 kJ mol^{-1}), and in part

DOI: 10.1021/jacs.6b03749
J. Am. Chem. Soc. 2016, 138, 8194−8206

Table 3. Energies (in kJ mol^{-1}), Main Configurations and Oscillator Strengths Calculated for Each Local Minimum Structure of BDAA-methyl at the TD-B3LYP/6-31+G(d) Level[a]

structure		S_0	S_1	S_2	S_3	$E_1 - E_0$
S0MIN1	C_{2h}	0.0	290.22	291.70	298.28	290.22
			[0.99n → π^*]	[0.99n → π^*]	[0.98π → π^*]	(412 nm)
			0.0000	0.0000	0.1042	(24 300 cm^{-1})
S0MIN2	C_{2v}	0.50	289.45	292.45	298.34	288.95
			[0.99n → π^*]	[0.99n → π^*]	[0.98π → π^*]	(414 nm)
			0.0000	0.0000	0.1033	(24 200 cm^{-1})
S1MIN1	C_s	37.98	245.88	305.66	309.70	207.90
			[0.99n → π^*]	[0.99n → π^*]	[0.99π → π^*]	(576 nm)
			0.0000	0.0000	0.1019	(17 400 cm^{-1})
S1MIN2	C_{2h}	27.56	237.96	336.11	351.48	210.40
			[0.99(n + π) → π^*]	[0.99n → π^*]	[0.81(n + π) → π^*] + 0.18[π → π^*]	(569 nm)
			0.1151	0.0000	0.0605	(17 600 cm^{-1})

[a]Important MOs at each minimum are given in Figure S48−S51. Details of excited states in Table S6

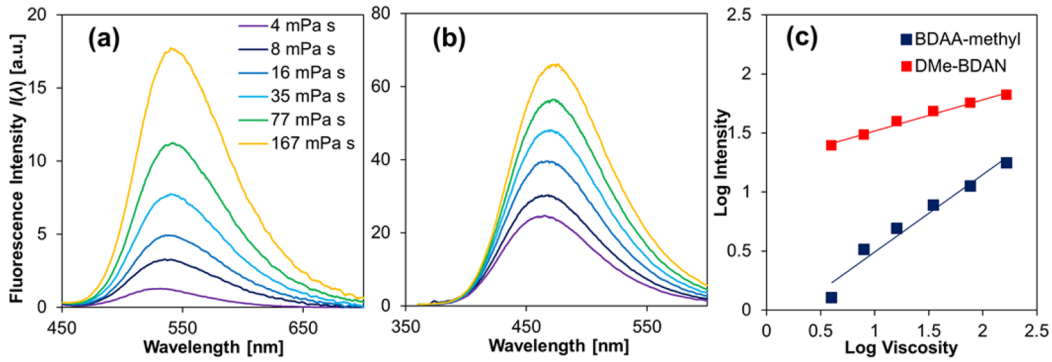

Figure 6. Fluorescence spectra of (a) **BDAA-methyl** and (b) **DMe-BDAN** in alcohol mixtures of different viscosity. (c) Peak fluorescence intensity plotted over solvent viscosity in a double-logarithmic scale. Experimental procedure was noted in Supporting Information (Section S1).[58]

from the destabilization of the ground state in the same geometry change (44 and 52 kJ mol^{-1}, respectively). Florescence frequencies from S1MIN1 and S1MIN2 are very similar to each other and we cannot tell which structure is more dominant. S1MIN2 is about 8 kJ mol^{-1} lower, and holds a larger oscillator strength (0.1151) than S1MIN1 (0.0). Therefore, S1MIN2 may be more important in gas phase or in solution.

However, one important problem is whether these structures are equally accessible in solid. In general, a large motion will be suppressed in the crystalline state (Figure 2 and 3). The S1MIN1 structure, compared to the Franck−Condon S0MIN1 or S0MIN2 structure, can be reached by planarization of only one amine group, and is not involved any large motion such as rotation or bending. On the other hand, S1MIN2 requires a large rotational motion (φ and φ' in Table 2) of the dialkylamine group in addition to planarization. Therefore, the molecule in solid is more likely to reach S1MIN1, but not to S1MIN2, and thus S1MIN1 plays a more important role in solid.

The resultant large Stokes shift suppresses the self-absorption (emission of one molecule absorbed by a neighboring molecule), and the small oscillator strength prevents each **BDAA** molecule from undesirable excitonic interactions with neighboring molecule. Avoiding self-absorption is one of the important requirements for efficient solid-state fluorescence. It is surprising and exciting that such primitive aromatic amines as **BDAAs** can achieve a large Stokes shift comparable to highly designed donor−acceptor systems.[44,45,50]

Experimental Observation of Nonradiative Transition.

In contrast to efficient solid-state fluorescence, **BDAAs** are nonfluorescent in solution state (Table 1). It is intriguing because 9,10-diphenylanthracene and some other 9,10-disubstituted anthracenes are well-known as highly fluorescent molecules, and are adopted as the standard for relative fluorescence quantum yield measurements.[51] In fact, **BDAA-propyl**, the most fluorescent **BDAA**, is quenched by nonradiative transition at the rate of ≈ 2 × 10^8 s^{-1} (Table S1), which is much faster than 9,10-diphenylanthracene (1 × 10^7 s^{-1}) and 9,10-dimethylanthracene (3 × 10^7 s^{-1}).[52] We previously investigated the effect of regioisomerism of **BDAAs** on their nonradiative transition rates.[21] It was revealed that the fast nonradiative transitions were activated only when dialkylamino groups were introduced at the 1,4- or 9,10-positions of anthracene, while other regioisomers of **BDAAs** are highly fluorescent due to slow nonradiative transitions (0.4−5 × 10^7 s^{-1}).[21] These fast nonradiative transitions are completely suppressed at 77 K (Table S3, Figure S36) without appearance of phosphorescence (Figure S37).

In addition, the viscosity dependence of $S_0 \leftarrow {}^1$CT fluorescence of 9-(*N*,*N*-dimethylamino)anthracene is reported by Warner et al.[20] In fact, fluorescence intensity of **BDAA-methyl** soared as solvent viscosity increased (Figure 6a). The fluorescence intensity $I(\lambda_f)$ of a molecular rotor follows the power-law relationship with viscosity η, as derived from Förster−Hoffmann equation,[53]

$$\log I(\lambda_f) = C + x \log \eta \quad (1)$$

DOI: 10.1021/jacs.6b03749
J. Am. Chem. Soc. 2016, 138, 8194−8206

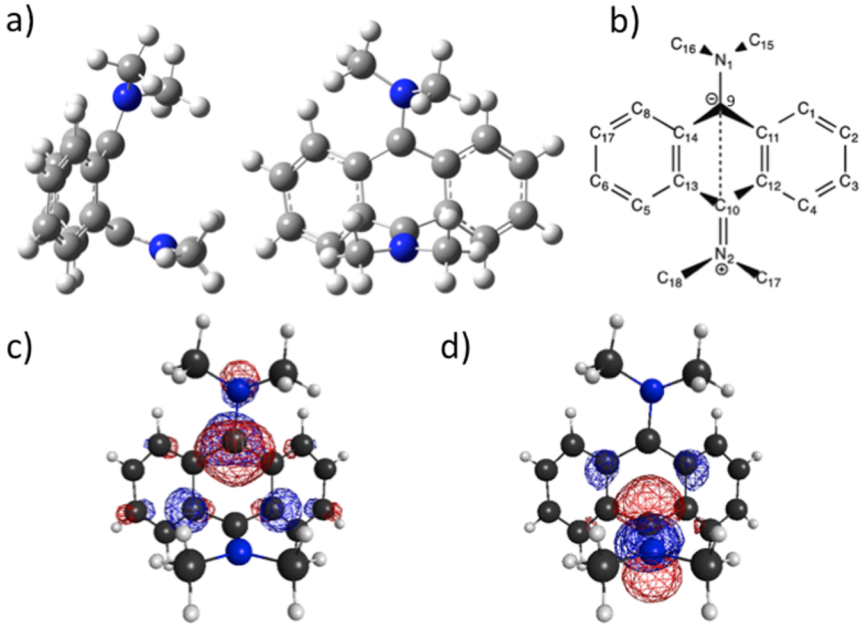

Figure 7. (a) Two views of the structure of located S_1/S_0 MECI of **BDAA-methyl** at the 2sa-CASSCF(10e/8o)/6-31G(d) level; (b) a simplified quinoidal resonance structure; and (c) and (d) two natural orbitals at the S_1/S_0 MECI of **BDAA-methyl** with occupation numbers of 1.45 and 0.52, respectively, for S_0−S_1 averaged density.

In this equation, C is a concentration- and temperature-dependent constant and x is a constant of each dye. For **BDAA-methyl** (Figure 6c, $R^2 = 0.96$) x is 0.66, which is comparable to the representative molecular rotor 9-(dicyanovinyl)-julolidine (**DCVJ**, $x = 0.53$),[54] thioflabin-T ($x = 0.72$),[55] and other highly viscosity-sensitive molecular rotors.[56,57] **BDAA-methyl** can be used as a molecular rotor, because it satisfies another requirement for molecular rotor such as absence of polarity effects on fluorescence quantum yield.[11]

It can be concluded from these experimental results that introduction of dialkylamino groups at the 1,4- or 9,10-positions of anthracene is the key strategy for fast internal conversions.

Calculated Conical Intersections. As discussed in the introduction, the nonadiabatic decay is controlled by the low energy conical intersections between the S_1 and S_0 states that are reachable with some vibrational motions (the reaction coordinate) from the Franck−Condon geometry. Therefore, we should find the structures and energies of low energy MECIs.

From previous experimental results,[21] the substitution by two dialkylamino groups at the *para*-positions is the key feature of this AIE. This suggests that an efficient decay path exists only for the *para*-substituted **BDAA**s, along the reaction is unique in the *para*-substituted arenes. We have already found that the amine planarization and aryl-nitrogen rotation can stabilize the excited state, and therefore stabilize some MECIs by delocalization of the π electrons. In addition, previous calculations showed that pyramidalization of one carbon on the arene rings of benzene, naphthalene and anthracene provides low energy MECIs.[59] Some preliminary calculations on benzene showed doubly pyramidalized benzene at the *para* position has an MECI (See Figure S53, Table S11−S12) with a Dewar-benzene type deformation, which would be suited ideally for conjugation with two sets of amine lone pairs. Guided by these ideas, we looked for low energy S_1/S_0 MECIs for **BDAA-methyl.**

In order to find MECI structures between the S_0 and S_1 states, we adopted the CASSCF(10e/8o)/6-31G(d) method with the active space consisting of nitrogen lone-pairs and the 6π electrons in the 6π orbitals on the central aromatic ring. MECI is optimized without consideration of explicit solvation. It is difficult to optimize MECI geometry in solution, because a large number of solvent coordinates increase dimensionality of potential energy surface in solution. Therefore, we base our discussion on gas phase calculations to understand the qualitative picture. There are advanced techniques to locate MECI in solution, in particular with quantum mechanics/molecular mechanics (QM/MM) methods, ab initio molecular dynamics methods,[60,61] continuum model[62] and reference interaction site model.[63−66] It is fascinating to discuss details about MECI with advanced techniques, but this is out of the scope of the present manuscript.

Starting with an approximate crossing point between S_0 and the lowest triplet state T_1,[67] an MECI of **BDAA-methyl** with a structure like Dewar-benzene was located, as shown in Figure 7a (also Table S13). The energies calculated at this level cannot be compared with those at the TD-DFT level in the preceding section. In Table 4, CASSCF/6-31G(d) energies of the MECI as well as of the DFT-optimized S0MIN1 are shown. The energy of the S_1 state at the MECI is 43.6 kJ mol^{-1} lower in energy than that at the Franck−Condon geometry. We do not

Table 4. Energies (in kJ mol^{-1}) Calculated for Each Structure of BDAA-methyl at the (10e/8o) CASSCF/6-31G(d) Level

structure		S_0	S_1	S_2	S_3
S0MIN1	C_{2h}	0.0	413.39	473.13	569.58
MECI[a]	C_1	364.03	368.98		

[a]Because of low convergence criterion used, energies of S_0 and S_1 states are not exactly the same.

DOI: 10.1021/jacs.6b03749
J. Am. Chem. Soc. 2016, 138, 8194−8206

discuss solvation effects carefully in this paper but preliminary results did not change the qualitative picture (See Table S15).

This MECI structure shows a quinoid biradical character, and has a structure similar to a minimum on the S_2 state of benzene,[68] as well as an MECI of benzene dipyramidalized at the *para* positions of benzene (Figure S53). Some key bond distances in Table 5 indicate clearly that the central benzene group has two short bonds corresponding to the quinoidal structure. Some dihedral angles in Table 5 (also seen in Figure 7a) also show that the central benzene ring is folded in a boat form. The C_{10} atom is planar, while the C_9 atom is nearly pyramidal. These structure features are consistent with the dominance of a quinoidal resonance structure shown in Figure 7b. Thus, one can say that the distortion to the Dewar-benzene like structure that accompany a large amplitude motion of amine groups, also seen clearly in Figure 7a, is the reaction or activation coordinate leading from the Franck−Condon structure to the MECI.

Table 5. Important Geometrical Parameters for MECI of BDAA-methyl at the 2sa-(10e/8o) CASSCF/6-31G(d) Level

	MECI	S0MIN1[a]
atom[b]	bond length [Å]	bond length [Å]
C_9C_{10}	2.48	2.83
$C_{11}C_{12}$	1.40	1.43
$C_{13}C_{14}$	1.41	1.43
$C_{10}N_2$	1.32	1.43
C_9N_1	1.44	1.43
atom[b]	dihedral angle [°]	dihedral angle [°]
$C_{13}C_{14}C_9C_{11}$	44.99	0
$C_{13}C_{14}C_{10}C_{12}$	62.57	180
$C_{13}C_5C_{10}N_2$	71.61	180
$C_8C_{14}C_9N_1$	29.35	0
atom[b]	dihedral angle [°]	
$C_{11}C_{14}C_9N_1$	156.24	180
$C_{12}C_{13}C_{10}N_2$	176.51	180

[a]Structure is optimized by (10e/8o) CASSCF/6-31G(d). Thus, structure is slightly different from DFT structure in Table S7. [b]Specification of atom labels is illustrated in Figure 7b.

In the liquid phase, fast internal conversion via this MECI should result in a low fluorescence quantum yield. On the other hand, such a large out-of-plane deformation required to reach the MECI is not allowed in the solid, because of the repulsion from closely stacked anthracene rings within the van der Waals radii (Figure 3). Thus, we conclude that the inability to reach MECI with large deformation in solid is responsible for steric-environment sensitivity of **BDAA**s.

In order to design steric-environment sensitive fluorophores, it is a good strategy to introduce certain substituent groups to control energy of the MECI. In this direction, calculations of MECI structure and its energy is the guiding tool. In the case of polycyclic aromatic hydrocarbons, MECI should be stabilized by introducing strong donors in the *para* positions.

Demonstration of the Design Strategy in Naphthalene Systems. So far, we have discussed the underlying mechanisms of aggregation-induced emission of **BDAA**s. Once we stabilize the MECI with a large deformation via *para* disubstitution by strong donors, fast internal conversion

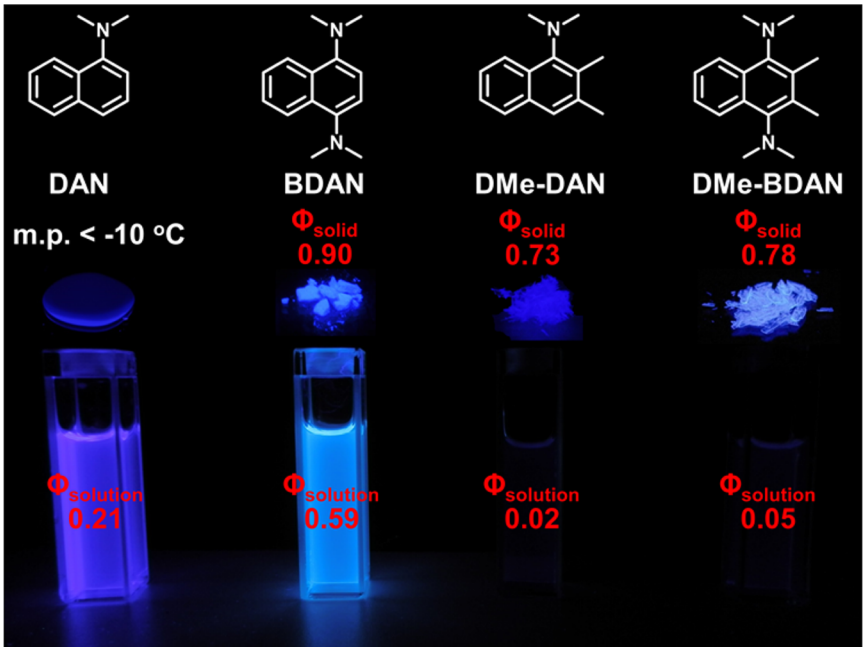

Figure 8. Fluorescence quantum yield of **DAN** and its derivatives in polycrystalline solids (Φ_{solid}) and in acetonitrile solution ($\Phi_{solution}$) with corresponding digital photographs taken under 365 nm irradiation.

DOI: 10.1021/jacs.6b03749
J. Am. Chem. Soc. 2016, 138, 8194−8206

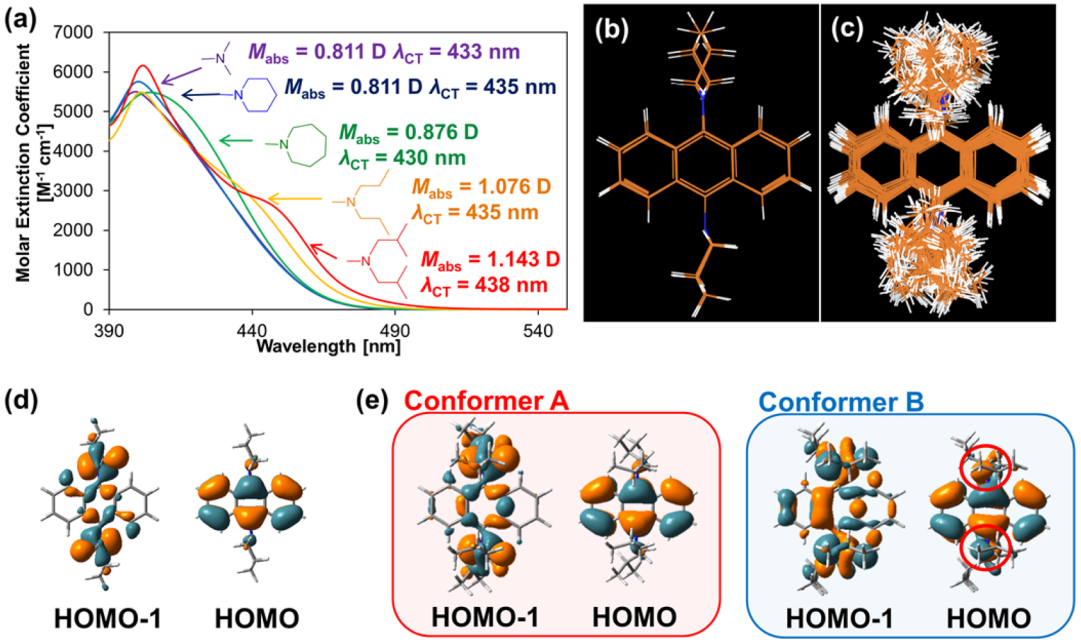

Figure 9. Effects of alkyl-chain flexibility on the $S_0 \rightarrow {}^1CT$ transition of BDAAs. (a) Absorption spectra of **BDAAs** (inset: transition moment M_{abs} [D] and maxima λ_{CT} of $S_0 \rightarrow {}^1CT$ absorption bands, which are discerned from $S_0 \rightarrow {}^1L_a$ absorption bands by Gaussian-fitting). Superpositions of low energy conformations (less than 12 kJ mol^{-1} from the global minima) of (b) **BDAA-6** and (c) **BDAA-isobutyl**. (d) HOMO and HOMO−1 of $n-\pi^*$ nonconjugative conformers of **BDAA-6**, and (e) those of $n-\pi^*$ nonconjugative (conformer A) and conjugate (conformer B) conformers of **BDAA-isobutyl**.

through the MECI takes place in the liquid phase, but strong AIE is achieved in solid. This design strategy can be applied for various aromatic hydrocarbons. Therefore, we have applied this strategy to activate AIE of naphthalene. 1-(*N*,*N*-dialkylamino)-naphthalene (**DAN**) and 1,4-bis(*N*,*N*-dialkylamino)-naphthalene (**BDAN**) are simple aromatic amines and their photophysics were well studied.[51,69−71] Their fluorescence properties were characterized by internal conversion, where polar environments[69,70] decelerate internal conversion and recover fluorescence intensity (Table S4). If MECIs of **DAN** and **BDAN** have similar structures as **BDAA-methyl**, fast internal conversion of **DAN** and **BDAN** would take place in liquid but not in solid. As expected, **BDAN** has exhibited moderate AIE (Figure 8), where fluorescence quantum yield in acetonitrile solution was 0.59 and increases up to 0.90 in polycrystalline solids (Table S4). The AIE effect become far more drastic when *N*,*N*-dialkylamino groups are twisted through the methyl groups at 2,3-positions. Both $S_0 \rightarrow {}^1CT$ absorption (Figure S38−S39) and $S_0 \leftarrow {}^1CT$ fluorescence (Figure S40−S41) of **DMe-DAN** and **DMe-BDAN** are severely forbidden in solution, but their fluorescence quantum yields are greatly enhanced in polycrystalline solids (Figure 8). Furthermore, **DMe-BDAN** exhibited the strong viscosity effect on fluorescence intensity in the same way with **BDAA-methyl** (Figure 6b). The performance as a molecular rotor was evaluated (Figure 6c) to be moderate (x = 0.27, refer eq 1), which was comparable to the molecular rotors recently reported as the fluorescence lifetime imaging agent.[72] More detailed analysis of AIE mechanism in **DMe-DAN** and **DMe-BDAN** lies outside the scope of the present study, and thus we just point out that *para* disubstitution by highly twisted *N*,*N*-dialkylamines is a promising design strategy for AIEgens and molecular rotors based on simple aromatic hydrocarbons. It is also noteworthy that both **DMe-DAN** and **DMe-BDAN** are smaller in terms of molecular weights than any other AIEgens reported so far.

Effects of Alkyl Chain Flexibility. As we described above, planarization of dialkylamine moieties (θ and θ') as well as the rotation (φ and φ') around the Ar−N bonds plays an important role in relaxation process of the S_1 excited state. Thus, we can easily imagine that different alkyl groups can make large differences in photophysical properties of **BDAAs**. UV−vis spectra of a variety of **BDAAs** actually showed significant differences. Generally speaking, the number of possible conformers corresponds to width of the absorption band. If there are only a few conformers, energy levels will be discreted, and therefore a sharp absorption band can be observed. If there are many conformers, absorption band can be broaden; in particular absorption with longer wavelength corresponding to less stable conformers will be enhanced.

As shown in Figure 9a, UV−vis spectra of **BDAAs** show the $S_0 \rightarrow {}^1L_a$ absorption bands that corresponds to the $S_0 \rightarrow S_3$ transition (Table 3) with maxima around 400 nm, and this is common for many 9,10-disubstituted anthracenes.[52] In addition, **BDAAs** possess small and hidden $S_0 \rightarrow {}^1CT$ absorption bands[20] around 430−440 nm, and are enhanced in polar environment, but vanished upon acidification (Figure S34). This feature suggests that the transition involves the *n*-orbitals on two nitrogen atoms. Since strength of the $S_0 \rightarrow {}^1CT$ absorption bands directly reflects the orbital overlap between the lone-pairs of nitrogen atoms and the π-orbitals of anthracenes, a comparison of the $S_0 \rightarrow {}^1CT$ absorption bands is a good indication of dihedral angle around the aryl-nitrogen bond of **BDAAs**. If the *n*-orbitals are perpendicular to the anthracene π-orbitals, transition dipole from the *n*-orbitals to the π^*-orbitals will be zero. When the *n*-orbitals mix with the π-orbitals, transition dipole has a finite value. Figure 9a shows larger transition dipole moments M_{abs} of $S_0 \rightarrow {}^1CT$ absorption for bulky **BDAA-propyl** and **BDAA-isobutyl** than compact

DOI: 10.1021/jacs.6b03749
J. Am. Chem. Soc. 2016, 138, 8194−8206

BDAA-methyl. Thus, the experimental results imply that bulky but more flexible **BDAA-propyl** and **BDAA-isobutyl** are more likely to take conformations with φ and $\varphi' \neq 0$ around their aryl-N bonds that allow conjugation of the *n*- and π^*-orbitals than the more compact but rigid **BDAA-methyl** and **BDAA-6**.

To clarify what makes the difference among these molecules, we have optimized local minima for the ground state of **BDAA-6** and **BDAA-isobutyl** at the B3LYP-D3/6-31G(d) level. For less flexible **BDAA-6**, only 2 local minima were found within 12 kJ mol^{-1} from the global minimum (Figure 9b). Both have pyramidal ($\theta \sim 146°$) and nonconjugative ($\varphi \sim 0$) amine structures, where HOMO and HOMO−1 do not mix (Figure 9d). On the other hand, for flexible **BDAA-isobutyl**, more than 90 conformations were found with within 12 kJ mol^{-1} from the global minimum (Figure 9c). The most low-energy conformers have nonconjugative ($\varphi \sim 0$) structures, where HOMO and HOMO−1 do not mix (conformer A in Figure 9e), while some of higher-energy conformers have conjugative ($\varphi \neq 0$) structures (conformer B in Figure 9e), in which lone-pairs on nitrogen atoms take part in π conjugation and result in $S_0 \rightarrow {}^1CT$ absorption around 400−430 nm. It is also worth noting that this absorption is allowed because disordered conformers have lower symmetry. This explains the low energy absorption peak around 400−430 nm in **BDAA-isobutyl** and **BDAA-propyl**.

Our experimental and theoretical studies revealed that the flexibility of alkyl chain dramatically increased the number of possible conformations. Rigid and compact group like dimethylamino and piperidyl group cannot move freely, and hindered by hydrogens atoms at 1, 4, 5, and 8 positions, while bulky but flexible diisobutylamino and dipropylamino groups can avoid these hydrogen atoms and allow participation of nitrogen lone-pairs in π conjugation.

CONCLUSIONS

We have studied the steric-environment sensitivity of fluorescence of 9,10-bis(*N*,*N*-dialkylamino)anthracenes (**BDAAs**). Steady-state spectra and quantum-yield measurements of a variety of **BDAAs** in solution, colloidal suspension, NaBr suspension, and polycrystalline solids indicate that **BDAAs** are nonfluorescent in the solution state, but some of them are highly fluorescent in solid state, despite dense face-to-face packing. Prominent Stokes shifts were also observed.

DFT calculations for **BDAA-methyl** show that the pyramidal amine groups are highly twisted ($\varphi \sim 0$) in the ground state (S_0). The nitrogen lone-pair orbitals cannot conjugate with the anthracene π orbitals, because they are orthogonal to each other. In the excited state, two local minima were found, in which one or both amine groups were planarized. Fluorescence takes place from S_1 excited state minima. Stability of the S_1 minima as well as destabilization of the S_0 state at these structures cause large Stokes shift. Experimental measurement of nonadiabatic transition rate indicates that *para* disubstitution by dialkylamino or strongly electron-donating groups promotes fast internal conversion. The internal conversion takes place via the nonadiabatic transition at the minimum energy conical intersection (MECI) between S_1 and S_0 states. The MECI has a Dewar-benzene-like structure. The MECI can be reached efficiently in the liquid phase, and facilitates fast internal conversion. However, a large amplitude motion, namely planarization of amine nitrogen atoms and rotation around the aromatic C−N bond, is required to reach this MECI. In the solid state, close packing prevents reaching this MECI, prohibits nonadiabatic transition and causes efficient aggregation-induced emission. This idea is used to find experimentally that naphthalene analogues are also efficient aggregation-induced fluorophores. The flexibility of alkyl chains on amino groups permit many conformational minima in the ground state and is found to be important for allowed charge-transfer transitions experimentally and theoretically.

It is surprising and exciting to see that even such simple aromatic hydrocarbons show steric-environment sensitivity. Three design strategies can be proposed to tune small aromatic hydrocarbons: (1) highly twisted *N*,*N*-dialkylamines, (2) substitution at the *para* positions, and (3) flexible alkyl groups. Since naphthalene and anthracene moieties are frequently found in various natural products, the insight derived from our study can be used to furnish these ubiquitous molecules with steric-environment sensitivity that can be used for potential applications in broad range of photofunctional molecules.

ASSOCIATED CONTENT

Supporting Information

The Supporting Information is available free of charge on the ACS Publications website at DOI: 10.1021/jacs.6b03749.

Detailed synthetic procedures, NMR spectra, crystallographic information, photophysical data, and quantum-chemical calculations (PDF)
Crystal data of **BDAA-6** (CIF)
Crystal data of **BDAA-7** (CIF)
Crystal data of **BDAA-isobutyl** (CIF)
Crystal data of **BDAA-methyl** (CIF)
Crystal data of **BDAA-propyl** (CIF)

AUTHOR INFORMATION

Corresponding Authors

*morokuma.keiji.3a@kyoto-u.ac.jp
*konishi.g.aa@m.titech.ac.jp

Notes

The authors declare no competing financial interest.

ACKNOWLEDGMENTS

We appreciate Mr. Hirohiko Watanabe and Dr. Kiyotada Hosokawa (Hamamatsu photonics K.K.) for the use of Fluorescence Lifetime Spectrometer Quantaurus-Tau C11367-01 and Dewar flask holder for low temperature measurement A11238-04. This work was partially supported by grant-in-aid for Scientific Research (No. 15H02158) to KM at Kyoto University. The Computer resources at the Academic Center for Computing and Media Studies (ACCMS) at Kyoto University and Research Center of Computer Science (RCCS) at the Institute for Molecular Science are also acknowledged.

REFERENCES

(1) Cao, K.; Farahi, M.; Dakanali, M.; Chang, W. M.; Sigurdson, C. J.; Theodorakis, E. A.; Yang, J. *J. Am. Chem. Soc.* **2012**, *134*, 17338−17341.
(2) Goh, W. L.; Lee, M. Y.; Joseph, T. L.; Quah, S. T.; Brown, C. J.; Verma, C.; Brenner, S.; Ghadessy, F. J.; Tao, Y. N. *J. Am. Chem. Soc.* **2014**, *136*, 6159−6162.
(3) Yang, Z.; Cao, J.; He, Y.; Yang, J. H.; Kim, T.; Peng, X.; Kim, J. S. *Chem. Soc. Rev.* **2014**, *43*, 4563−4601.
(4) Okamoto, A.; Tainaka, K.; Nishiza, K.; Saito, I. *J. Am. Chem. Soc.* **2005**, *127*, 13128−13129.
(5) Priestley, R. D.; Ellison, C. J.; Broadbelt, L. J.; Torkelson, J. M. *Science* **2005**, *309*, 456−459.

DOI: 10.1021/jacs.6b03749
J. Am. Chem. Soc. 2016, 138, 8194−8206

(6) Ciardelli, F.; Ruggeri, G.; Pucci, A. *Chem. Soc. Rev.* **2013**, *42*, 857−870.
(7) Tang, T-Y. D.; Hak, R. C.; Thompson, A. J.; Kuimova, M. K.; Williams, D. S.; Perriman, A. W.; Mann, S. *Nat. Chem.* **2014**, *6*, 527−533.
(8) Shustova, N. B.; McCarthy, B. D.; Dinca, M. *J. Am. Chem. Soc.* **2011**, *133*, 20126−20129.
(9) Suhina, T.; Weber, B.; Carpentier, C. E.; Lorincz, K.; Schall, P.; Bonn, D.; Brouwer, A. M. *Angew. Chem., Int. Ed.* **2015**, *54*, 3688−3691.
(10) Mustafic, A.; Huang, H.-M.; Theodorakis, E. A.; Haidekker, M. A. *J. Fluoresc.* **2010**, *20*, 1087−1098.
(11) Haidekker, M. A.; Theodorakis, E. A. *Org. Biomol. Chem.* **2007**, *5*, 1669−1678.
(12) Mei, J.; Hong, Y.; Lam, J. W. Y.; Qin, A.; Tang, Y.; Tang, B. Z. *Adv. Mater.* **2014**, *26*, 5429−5479.
(13) Amdursky, N.; Erez, Y.; Huppert, D. *Acc. Chem. Res.* **2012**, *45*, 1548−1557.
(14) Zhu, L.; Zhao, Y. *J. Mater. Chem. C* **2013**, *1*, 1059−1065.
(15) Hu, R.; Lager, E.; Aguilar, A. A.; Liu, J.; Lam, J. W. Y.; Sung, H. H. Y.; Williams, I. D.; Zhong, Y.; Wong, K. S.; Cabrera, E. P.; Tang, B. Z. *J. Phys. Chem. C* **2009**, *113*, 15845−15853.
(16) (a) Grabowski, Z. R.; Rotkiewicz, K.; Rettig, W. *Chem. Rev.* **2003**, *103*, 3899−4031. (b) Sasaki, S.; Drummen, G. P. C.; Konishi, G. *J. Mater. Chem. C* **2016**, *4*, 2731−2743.
(17) Li, Q.; Blancafort, L. *Chem. Commun.* **2013**, *49*, 5966−5968.
(18) Blancafort, L. *ChemPhysChem* **2014**, *15*, 3166−3181.
(19) Zhang, T.; Jiang, Y.; Niu, Y.; Wang, D.; Peng, Q.; Shuai, Z. *J. Phys. Chem. A* **2014**, *118*, 9094−9108.
(20) Day, J.; Warner, I. M. *J. Phys. Chem. A* **1997**, *101*, 4872−4878.
(21) Sasaki, S.; Igawa, K.; Konishi, G. *J. Mater. Chem. C* **2015**, *3*, 5940−5950.
(22) (a) Bernardi, F.; Olivucci, M.; Robb, M. A. *Chem. Soc. Rev.* **1996**, *25*, 321−328. (b) Yarkony, D. R. *Acc. Chem. Res.* **1998**, *31*, 511−518.
(23) Ruiz-Barragan, S.; Morokuma, K.; Blancafort, L. *J. Chem. Theory Comput.* **2015**, *11*, 1585−1594.
(24) Suzuki, S.; Maeda, S.; Morokuma, K. *J. Phys. Chem. A* **2015**, *119*, 11479−11487.
(25) Peng, X.-L.; Ruiz-Barragan, S.; Li, Z.-S.; Li, Q.-S.; Blancafort, L. *J. Mater. Chem. C* **2016**, *4*, 2802−2810.
(26) (a) Levine, B. G.; Ko, C.; Quenneville, J.; Martinez, T. J. *Mol. Phys.* **2006**, *104*, 1039−1051. (b) Levine, B. G.; Coe, J. D.; Martinez, T. J. *J. Phys. Chem. B* **2008**, *112*, 405−413.
(27) Bearpark, M. J.; Robb, M. A.; Schlegel, H. B. *Chem. Phys. Lett.* **1994**, *223*, 269−274.
(28) Maeda, S.; Ohno, K.; Morokuma, K. *J. Chem. Theory Comput.* **2010**, *6*, 1538−1545.
(29) Wolfe, J. P.; Wagaw, S.; Buchwald, S. L. *J. Am. Chem. Soc.* **1996**, *118*, 7215−7216.
(30) Suzuki, Y.; Fukui, N.; Murakami, K.; Yorimitsu, H.; Osuka, A. *Asian J. Org. Chem.* **2013**, *2*, 1066−1071.
(31) Chung, Y.; Duerr, B. F.; Mckelvey, T. A.; Nanjappan, P.; Czarnik, A. W. *J. Org. Chem.* **1989**, *54*, 1018−1032.
(32) Campbell, T. W.; Mccoy, V. E.; Kauer, J. C.; Foldi, V. S. *J. Org. Chem.* **1961**, *26*, 1422−1426.
(33) Charles, M. D.; Schultz, P.; Buchwald, S. L. *Org. Lett.* **2005**, *7*, 3965−3968.
(34) Prashad, M.; Mak, X. Y.; Liu, Y.; Repic, O. *J. Org. Chem.* **2003**, *68*, 1163−1164.
(35) Riedmuller, S.; Kaufhold, O.; Spreizer, H.; Nachtsheim, B. J. *Eur. J. Org. Chem.* **2014**, *2014*, 1391−1394.
(36) Robinson, S. R.; Wells, C. H. J. *Tetrahedron* **1973**, *29*, 2203−2207.
(37) Sorokin, V. I.; Ozeryanskii, V. A.; Pozharskii, A. F. *Eur. J. Org. Chem.* **2003**, *2003*, 496−498.
(38) Frisch, M. J.; Trucks, G. W.; Schlegel, H. B.; Scuseria, G. E.; Robb, M. A.; Cheeseman, J. R.; Scalmani, G.; Barone, V.; Mennucci, B.; Petersson, G. A.; Nakatsuji, H.; Caricato, M.; Li, X.; Hratchian, H. P.; Izmaylov, A. F.; Bloino, J.; Zheng, G.; Sonnenberg, J. L.; Hada, M.; Ehara, M.; Toyota, K.; Fukuda, R.; Hasegawa, J.; Ishida, M.; Nakajima, T.; Honda, Y.; Kitao, O.; Nakai, H.; Vreven, T.; Montgomery, J. A., Jr.; Peralta, J. E.; Ogliaro, F.; Bearpark, M.; Heyd, J. J.; Brothers, E.; Kudin, K. N.; Staroverov, V. N.; Kobayashi, R.; Normand, J.; Raghavachari, K.; Rendell, A.; Burant, J. C.; Iyengar, S. S.; Tomasi, J.; Cossi, M.; Rega, N.; Millam, J. M.; Klene, M.; Knox, J. E.; Cross, J. B.; Bakken, V.; Adamo, C.; Jaramillo, J.; Gomperts, R.; Stratmann, R. E.; Yazyev, O.; Austin, A. J.; Cammi, R.; Pomelli, C.; Ochterski, J. W.; Martin, R. L.; Morokuma, K.; Zakrzewski, V. G.; Voth, G. A.; Salvador, P.; Dannenberg, J. J.; Dapprich, S.; Daniels, A. D.; Farkas, Ö.; Foresman, J. B.; Ortiz, J. V.; Cioslowski, J.; Fox, D. J. *Gaussian 09*, Revision D.01; Gaussian, Inc.: Wallingford, CT, 2009.
(39) (a) Schmidt, M. W.; Baldridge, K. K.; Boatz, J. A.; Elbert, S. T.; Gordon, M. S.; Jensen, J. H.; Koseki, S.; Matsunaga, N.; Nguyen, K. A.; Su, S. J.; Windus, T. L.; Dupuis, M.; Montgomery, J. *J. Comput. Chem.* **1993**, *14*, 1347. (b) Gordon, M. S.; Schmidt, M. W. Advances in electronic structure theory: GAMESS a decade later. In *Theory and Applications of Computational Chemistry: The First Forty Years*; Dykstra, C. E., Frenking, G., Kim, K. S., Scuseria, G. E., Eds.; Elsevier: Amsterdam, The Netherlands, 2005; p 1167.
(40) Ponder, J. W.; Richards, F. M. *J. Comput. Chem.* **1987**, *8*, 1016−1024.
(41) (a) Allinger, N. L.; Yuh, Y. H.; Lii, J.-H. *J. Am. Chem. Soc.* **1989**, *111*, 8551−8566. (b) Lii, J.-H.; Allinger, N. L. *J. Am. Chem. Soc.* **1989**, *111*, 8566−8575. (c) Lii, J.-H.; Allinger, N. L. *J. Am. Chem. Soc.* **1989**, *111*, 8576−8582.
(42) Dong, Y.; Lam, J. W. Y.; Qin, A.; Sun, J.; Liu, J.; Li, Z.; Zhang, S.; Sun, J.; Kwok, H. S.; Tang, B. Z. *Appl. Phys. Lett.* **2007**, *91*, 011111.
(43) Chen, M.; Li, L.; Nie, H.; Tong, J.; Yan, L.; Xu, B.; Sun, J. Z.; Tian, W.; Zhao, Z.; Qin, A.; Tang, B. Z. *Chem. Sci.* **2015**, *6*, 1932−1937.
(44) Schill, H.; Nizamov, S.; Bottanelli, F.; Bierwagen, J.; Belov, V. N.; Hell, S. W. *Chem. - Eur. J.* **2013**, *19*, 16556−16565.
(45) Araneda, J. F.; Piers, W. E.; Heyne, B.; Parvez, M.; McDonald, R. *Angew. Chem., Int. Ed.* **2011**, *50*, 12214−12217.
(46) (a) Lippert, E. L. *Organic Molecular Photophysics*; Wiley: New York, 1975. (b) Mataga, N.; Kubota, T. *Molecular Interaction and Electronic Spectra*; Dekker: New York, 1970.
(47) Montalti, M.; Credi, A.; Prodi, L.; Gandolfi, M. T. *Handbook of Photochemistry*; Taylor & Francis: Boca Raton, 2006, pp 536−540.
(48) Platt, J. R. *J. Chem. Phys.* **1949**, *17*, 484−495.
(49) (a) Kasha, M. *Discuss. Faraday Soc.* **1950**, *9*, 14−19. (b) Robinson, G. W.; Frosch, R. P. *J. Chem. Phys.* **1962**, *37*, 1962−1973. (c) Robinson, G. W.; Frosch, R. P. *J. Chem. Phys.* **1963**, *38*, 1187−1203.
(50) Sasaki, S.; Niko, Y.; Klymchenko, A. S.; Konishi, G. *Tetrahedron* **2014**, *70*, 7551−7559.
(51) Suzuki, K.; Kobayashi, A.; Kaneko, S.; Takehira, K.; Yoshihara, T.; Ishida, H.; Shiina, Y.; Oishi, S.; Tobita, S. *Phys. Chem. Chem. Phys.* **2009**, *11*, 9850−9860.
(52) Nijegorodov, N.; Mabbs, R. *Spectrochim. Acta, Part A* **2000**, *56*, 2157−2166.
(53) Förster, Th.; Hoffmann, G. *Z. Phys. Chem.* **1971**, *75*, 63−76.
(54) Haidekker, M. A.; Brady, T. P.; Lichltyter, D.; Theodorakis, E. A. *Bioorg. Chem.* **2005**, *33*, 415−425.
(55) Chatterjee, A.; Seth, D. *Photochem. Photobiol. Sci.* **2013**, *12*, 369−383.
(56) Levitt, J. A.; Chung, P.−H.; Kuimova, M.; Yahioglu, G.; Wang, Y.; Qu, J.; Suhling, K. *ChemPhysChem* **2011**, *12*, 662−672.
(57) Karpenko, I. A.; Niko, Y.; Yakubovskyi, V. P.; Gerasov, A. O.; Bonnet, D.; Kovtun, Y. P.; Klymchenko, A. S. *J. Mater. Chem. C* **2016**, *4*, 3002−3009.
(58) Kocsis, L. S.; Elbel, K. M.; Hardigree, B. A.; Brummond, K. M.; Haidekker, M. A.; Theodorakis, E. A. *Org. Biomol. Chem.* **2015**, *13*, 2965−2973.
(59) Harabuchi, Y.; Taketsugu, T.; Maeda, S. *Phys. Chem. Chem. Phys.* **2015**, *17*, 22561−22565.
(60) Toniolo, A.; Granucci, G.; Martinez, T. J. *J. Phys. Chem. A* **2003**, *107*, 3822−3830.

DOI: 10.1021/jacs.6b03749
J. Am. Chem. Soc. 2016, 138, 8194−8206

(61) Ortiz-Sanchez, J. M.; Bucher, D.; Pierce, L. C. T.; Markwick, P. R. L.; McCammon, A. J. *J. Chem. Theory Comput.* **2012**, *8*, 2752−2761.
(62) Burghardt, I.; Cederbaum, L. S.; Hynes, J. T. *Faraday Discuss.* **2004**, *127*, 395−411.
(63) Yamazaki, S.; Kato, S. *J. Chem. Phys.* **2005**, *123*, 114510.
(64) Mori, T.; Nakano, K.; Kato, S. *J. Chem. Phys.* **2010**, *133*, 064107.
(65) Minezawa, N. *Chem. Phys. Lett.* **2014**, *608*, 140−144.
(66) Minezawa, N. *J. Chem. Phys.* **2014**, *141*, 164118.
(67) In common practice, energy of the S_0, S_1, and T_1 states at the FC region follow the order of $S_0 < T_1 < S_1$. When the system approaches to the MECI, energies of the three states follow the order of $T_1 < S_0 = S_1$. Therefore, S_0/T_1 minimum energy seam crossing (MESC), in principle, energetically lower and closer to the S_0/S_1 MECI. Locating S_0/T_1 MESC is relatively straightforward, and this can be used as the starting point to located the S_0/T_1 MESC. In this study, we have used this strategy to locate S_0/S_1 MECI.
(68) Palmer, I. J.; Ragazos, I. N.; Bernardi, F.; Olivucci, M.; Robb, M. A. *J. Am. Chem. Soc.* **1993**, *115*, 673−682.
(69) Takehira, K.; Suzuki, K.; Hiratsuka, H.; Tobita, S. *Chem. Phys. Lett.* **2005**, *413*, 52−58.
(70) Sun, X.; Wen, Z.-C.; Jiang, Y.-B. *Spectrochim. Acta, Part A* **2007**, *68*, 220−224.
(71) Suzuki, K.; Demeter, A.; Kuhnle, W.; Tauer, E.; Zachariasse, K. A.; Tobita, S.; Shizuka, H. *Phys. Chem. Chem. Phys.* **2000**, *2*, 981−991.
(72) Peng, X.; Yang, Z.; Wang, J.; Fan, J.; He, Y.; Song, F.; Wang, B.; Sun, S.; Qu, J.; Qi, J.; Yan, M. *J. Am. Chem. Soc.* **2011**, *133*, 6626−6635.

DOI: 10.1021/jacs.6b03749
J. Am. Chem. Soc. 2016, 138, 8194−8206